buildings

MDPI

Article

Numerical Simulation of the Dynamic Responses and Impact-Bearing Capacity of CFDST Columns under Lateral Impact

Jin-Long Guo [1,2,3], Shuang Pan [1,4,*], Xiao Guo [2] and Zheng-Yu Wu [1,3]

[1] School of Engineering, Fujian Jiangxia University, Fuzhou 350108, China
[2] CSCEC Strait Construction Strait Construction and Development Co., Ltd., Fuzhou 350001, China
[3] Institute of Infrastructural Protection, Fujian Jiangxia University, Fuzhou 350108, China
[4] College of Transportation and Civil Engineering, Fujian Agriculture and Forestry University, Fuzhou 350108, China
* Correspondence: panshuang2279@163.com; Tel.: +86-13409856021

Abstract: The concrete-filled double steel tube (CFDST) has been more and more widely used in infrastructure due to its greater moment of inertia compared to the ordinary concrete-filled steel tube (CFST). With the increase in collision accidents occurring in recent years, the research on CFDST under impact needs more attention. To study the dynamic responses of CFDST columns under lateral impact, the finite element package ABAQUS was used to simulate the impact force and mid-span deflection of the column under the coupling action of axial force and lateral impact based on the comparison of experimental data in the literature. The influence of hollow ratio, axial compression ratio, slenderness ratio, impact energy, and material strength on the dynamic responses of the CFDST column are studied. The results show that with the increase in the hollow ratio from 0.3 to 0.8, the residual mid-span deflection of the CFDST column decreases by 77.9%. The mid-span deflection shows an increasing trend following a decreasing one with the axial compression ratio increasing. With the increase in the slenderness ratio from 30 to 60, the plateau impact force decreases by 62.5%, and the residual mid-span deflection increases by 240.5%. The practical formulas for the impact-bearing capacity and residual mid-span deflection of the CFDST column are suggested with high accuracy.

Keywords: numerical simulation; dynamic responses; impact-bearing capacity; concrete-filled double steel tube (CFDST); lateral impact; finite element method

Citation: Guo, J.-L.; Pan, S.; Guo, X.; Wu, Z.-Y. Numerical Simulation of the Dynamic Responses and Impact-Bearing Capacity of CFDST Columns under Lateral Impact. *Buildings* **2023**, *13*, 805. https://doi.org/10.3390/buildings13030805

Academic Editors: Yue-Ling Long, Zhenhao Zhang, Ying Qin, Zhiliang Zuo, JinJing Liao and Nerio Tullini

Received: 1 March 2023
Revised: 14 March 2023
Accepted: 15 March 2023
Published: 18 March 2023

1. Introduction

The concrete-filled double steel tube (CFDST) column is composed of inner and outer steel tubes with concrete between the two tubes. Compared with the ordinary concrete-filled steel tube column, the CFDST column has a greater moment of inertia in mechanics under the same cross-sectional area, so it has been more and more widely used in infrastructure. Researchers have carried out a series of studies on the mechanical properties of CFDST columns. For example, Huang et al. [1] carried out studies on the axial compression performance of the CFDST short column, with the hollow ratio as the main parameter. The result shows that the failure mode of the CFDST short column with a large hollow ratio is mainly shear failure with bulging deformation at the end. In addition, Yu et al. [2] carried out studies on the axial compression performance of the CFDST short column under fire. The columns are different in the sections, in terms of a square or circular hollow Sulthana et al. [3] found that the contribution of the inner tube is less than predicted in the axial compression-bearing capacity of the CFDST column, so a reduction coefficient is proposed to consider the real contribution of the inner tube.

On the other hand, collision accidents have occurred frequently in recent years, such as buildings being hit by vehicles or aircraft, bridges being hit by ships, and the shield structures beside mountains being hit by falling rock. The columns are laterally impacted in the collision accidents and always fail, or even collapse, which always leads to heavy losses and negative social influence. Researchers have carried out several studies on the lateral impact responses of the CFDST column or the ordinary concrete-filled steel tube (CFST) members. Hou et al. [4] carried out lateral impact testing of CFST column members, and the impact force, mid-span deflection, and failure mode of the members were analyzed. Feng et al. [5] conducted lateral continuous impact resistance testing of cantilever square weathering CFST columns and compared it with that of the normal CFST. Wang et al. [6] conducted a study on the CFST column to composite beam connection under impact, and investigated the dynamic increase factors based on force, deflection, and energy with various impact energies. Wang et al. [7] conducted lateral impact testing on conical and cylindrical CFDST members compared with the ordinary concrete-filled steel tube to reveal the dynamic process of different cross-section members. The results show that under the same impact energy, CFDST members can absorb higher energy with less deformation. Shi et al. [8] studied the mechanical properties of CFDST members with different outer steel tube materials under single and continuous impact tests, and found that the member with the stainless steel outer tube has more advantages in terms of resisting the impact under low-energy continuous impact. Wang et al. [9] found that the impact resistance of CFDST members is related to the hollow ratio by test, and the impact resistance is reduced when the hollow ratio exceeds a certain range. However, the CFDST specimens have no axial force in the above impact tests, which is not the same as the actuality of the column. Alongside the tests, numerical simulation is also an effective method to study the CFDST column under impact. An et al. [10] established an axial force–impact coupling model of CFDST members by using finite element software, and focused on the influence of the CFDST axial compression ratio and section steel ratio on the impact resistance of the members. Aghdamy et al. [11] analyzed the failure mode, impact force, and deformation of CFDST members with different axial loads under lateral impact by numerical simulation. In addition, there are many research works about concrete structure under impact or explosion using numerical simulation. Kang et al. [12] developed a modeling method that includes a contact model using mass–spring–damper elements to describe the contact behavior between the impactor and the CFST columns, and a nonlinear fiber-based beam–column element model to simulate the behavior of CFST columns under impact. Jahami et al. [13] numerically studied the effect of using CFRP as a strengthening technique for RC beams subjected to explosion. Wu et al. [14] applied numerical simulations based on the Arbitrary Lagrangian–Eulerian elements method to analyze the dynamic responses of ultra-high-performance cementitious composite-filled steel tube members subjected to explosion.

To sum up, although CFDST columns under static axial compression and lateral impact have been studied, there is still a lack of systematic analysis on the dynamic responses of CFDST columns under the coupling action of axial force and lateral impact. In the existing relevant literature, only a few factors have been analyzed, and the practical formulas for calculating the impact-bearing capacity and the deflection of the CFDST columns are relatively rare. Therefore, in this paper, the axial force–impact coupling model of CFDST columns is developed by using ABAQUS software, and the effects of hollow ratio, axial compression ratio, slenderness ratio, impact energy, and material strength on the lateral impact dynamic responses of the CFDST columns are discussed. In addition, practical formulas for calculating the impact-bearing capacity and the mid-span deflection of the CFDST columns are put forward.

2. Numerical Model

2.1. Material Model

2.1.1. Concrete

A 3D numerical model of the CFDST column was established by using the finite element package ABAQUS to simulate the dynamic responses of the column under the coupling action of axial force and lateral impact. The plastic damage model was adopted for the core concrete, between the outer and inner steel tubes, under uniaxial compression and tension. The compressive stress–strain relationship for concrete suggested by Han et al. [15] was used as below:

$$y = \begin{cases} 2x - x^2, & x \leqslant 1 \\ \dfrac{x}{\beta_0 (x-1)^{\eta} + x}, & x > 1 \end{cases} \tag{1}$$

where $y = \sigma/\sigma_0$, $x = \varepsilon/\varepsilon_0$, $\beta_0 = 0.5 \times \left(2.36 \times 10^{-5}\right)^{[0.25+(\xi-0.5)^7]} (f_c')^{0.5} \geqslant 0.12$, and $\eta = 2$. The $\sigma_0 = f_c'$, in which f_c' is the cylindrical compressive strength of concrete. The $\varepsilon_0 = \varepsilon_c + 800 \cdot \xi^{0.2} \cdot 10^{-6}$, in which $\varepsilon_c = (1300 + 12.5 \cdot f_c') \cdot 10^{-6}$ and $\xi = \frac{A_{so} \cdot f_{yo}}{A_{c,n} \cdot f_{ck}}$. A_{so} and f_{yo} are the cross-sectional area and yield strength of the outer steel tube. $A_{c,n}$ and f_{ck} are the cross-sectional area and standard compressive strength of concrete.

The tensile stress–strain relationship for concrete suggested by Han et al. [15] was used as below:

$$y = \begin{cases} 1.2x - 0.2x^6, & x \leqslant 1 \\ \dfrac{x}{0.31\sigma_p^2 (x-1)^{1.7} + x}, & x > 1 \end{cases} \tag{2}$$

where $y = \sigma_c/\sigma_p$, $x = \varepsilon_c/\varepsilon_p$, $\sigma_p = 0.26 \times (1.25 f_c')^{2/3}$, and $\varepsilon_p = 43.1\sigma_p(\mu\varepsilon)$. σ_p is the peak tensile stress of concrete and ε_p is the corresponding strain.

The elastic modulus was calculated as $4700\sqrt{f_c'}$ [16]. The parameters of the concrete model were set as shown in Table 1 [17].

Table 1. Material parameters of concrete.

ν	ρ/(kg·m^{-3})	e	a_f	K_c	$\mu/10^{-3}$	φ/(°C)
0.2	2500	0.1	1.16	2/3	1	30

The concrete strength would be increased under impact considering the rate effect. The dynamic increase factor of the concrete compressive strength was adopted based on the literature [18], and is shown below:

$$\mathrm{CDIF} = \frac{f_d}{f_{cm}} = \left(\dot{\varepsilon}_d/\dot{\varepsilon}_s\right)^{1.026\alpha}, \ \dot{\varepsilon}_d \leq 30\mathrm{s}^{-1} \tag{3}$$

where f_d is the dynamic compression strength when the strain rate is $\dot{\varepsilon}_d$, f_{cm} is the static compression strength, $\dot{\varepsilon}_s$ is the quasi-static strain rate in compression, and the value is -30×10^{-6}/s; and $\alpha = 1/(5 + 9(f_{cm}/f_{cm0}))$, in which the value of f_{cm0} is 10 MPa. The dynamic increase factor of the concrete tensile strength adopted is shown below [18]:

$$\begin{aligned} \mathrm{TDIF} &= \frac{f_{td}}{f_{ctm}} = \left(\dot{\varepsilon}_{dt}/\dot{\varepsilon}_{st}\right)^{\delta}, \ \dot{\varepsilon}_{dt} \leq 1\mathrm{s}^{-1} \\ \mathrm{TDIF} &= \frac{f_{td}}{f_{ctm}} = \beta_s \left(\dot{\varepsilon}_{dt}/\dot{\varepsilon}_{st}\right)^{1/3}, \ \dot{\varepsilon}_{dt} > 1\mathrm{s}^{-1} \end{aligned} \tag{4}$$

where f_{td} is the dynamic tensile strength when the strain rate is $\dot{\varepsilon}_{dt}$, f_{ctm} is the static tensile strength, $\dot{\varepsilon}_{st}$ is the quasi-static strain rate in tension, and the value is 1×10^{-6}/s, $\delta = 1/(1 + 8 f_{cm}/f_{cm0})$, and $\lg\beta_s = 6\delta - 2$.

2.1.2. Steel

The elastoplastic model based on the von Mises yield criterion was adopted for the steel tube. The stress–strain relationship for steel suggested by Han et al. [19] was used as shown in Figure 1, where f_p, f_y, and f_u are the proportioned limit, yield strength, and ultimate strength of the steel. In addition, $\varepsilon_1 = 0.8f_y/E_s$, $\varepsilon_2 = 1.5\varepsilon_1$, $\varepsilon_3 = 10\varepsilon_y$, and $\varepsilon_u = 100\varepsilon_y$.

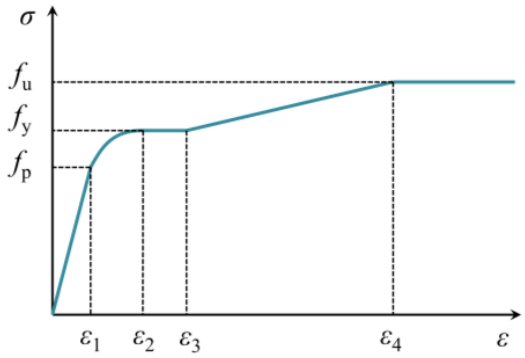

Figure 1. Stress–strain relationship for steel.

The parameters of the steel were set as listed in Table 2 [17]. In the same way as concrete, the steel strength would also be increased under impact. The dynamic increase factor of the steel strength was adopted by using the Cowper–Symonds model with the parameters given as $C = 6844/s$ and $p = 3.91$ [20], and is shown below:

$$\frac{f_y^d}{f_y} = 1 + \left(\frac{\dot{\varepsilon}}{C}\right)^{(1/p)} \quad (5)$$

where f_y^d is the dynamic yield strength when the strain rate is $\dot{\varepsilon}$ and f_y is the static yield stress.

Table 2. Material parameters of steel.

t/mm	ρ/(kg·m^{-3})	f_y/MPa	f_u/MPa	E_s/GPa	ν
3	7850	396	633.6	206	0.3

2.2. Element and Constraint

As shown in Figure 2, the numerical model is made up of the outer and inner steel tubes, the core concrete between the two tubes, the axial spring, and the impact mass. The steel tubes and concrete are created by the three-dimensional solid element, which has eight nodes with one-point Gauss integration. The impact mass is simplified as a rigid shell element. In order to ensure the consistent application of axial compressive force to the column, the axial spring is selected at the upper node of the column. The axial force is applied to the column by the compression spring to simulate the actual vertical load of the column. Surface-to-surface contact is adopted for the interaction between steel tubes and concrete, impact mass, and outer steel tube. The friction coefficient of Coulomb friction between the steel tubes and concrete is set as 0.6 [4] and the one between the impact mass and outer steel tube is 0, while hard contact is adopted in the normal direction of the contact interface.

The boundary condition of the column is set as the fixed constraint at both ends. To achieve it, the nodes in the two interfaces at both ends are bound to a respective point, and the bottom point is fixed in all directions, while the constraint at the top point is released in the axial direction displacement to exert the axial force conducted by the spring. The impact mass is free in the lateral direction but fixed in all other directions. The element size of 15 mm is adopted as the main element size for the concrete and steel tube in this study.

The impact mass is set as 10 mm beside the column to save on computational cost, and the initial velocity is added by the predefined field to simulate the impact.

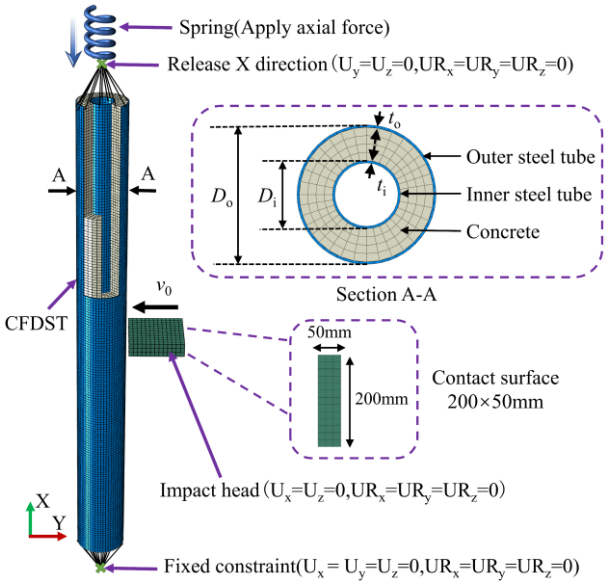

Figure 2. Numerical model of CFDST column.

The whole analysis process of the CFDST column under the coupling action of axial compression and lateral impact is divided into 3 steps, as shown in Figure 3. Firstly, the model of the CFDST column under axial compression only is established to obtain the axial ultimate bearing capacity of the member. Secondly, a general static analysis step is created, in which the axial force based on the ratio of axial compression is applied to the top end of the column. The axial force is caused by the corresponding compression displacement of the axial spring. The value of the axial force is equal to the arithmetic product of the ratio of axial compression and the ultimate bearing capacity obtained in the previous analysis step. Lastly, the model of CFDST column with axial compression under lateral impact is established, and an explicit dynamic analysis step is created. To simulate the axial compression state, the result of the general static analysis in the second step is imported into this explicit model as an initial stress field. Then, the CFDST column would be laterally impacted by the rigid mass.

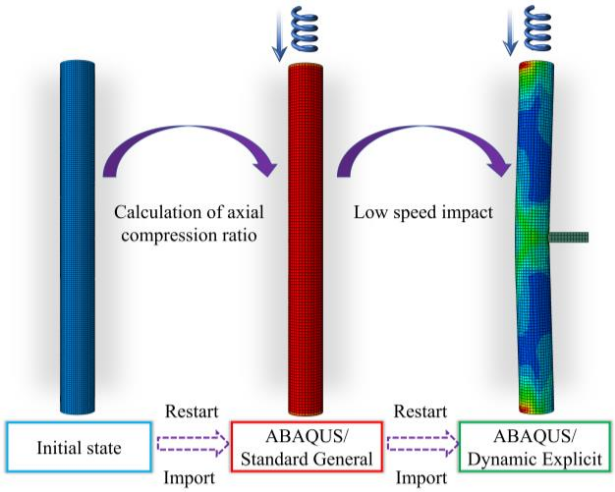

Figure 3. The whole analysis process.

2.3. Verification

The energy output result of the numerical model is an important index to evaluate the rationality of the simulation. Figure 4 shows the energy–time history curve of the whole model. The total energy of the whole model is essentially maintained at a fixed value, while the hourglass energy (ALLAE) is about 9% of the internal energy (ALLIE), which indicates that the numerical model is rational.

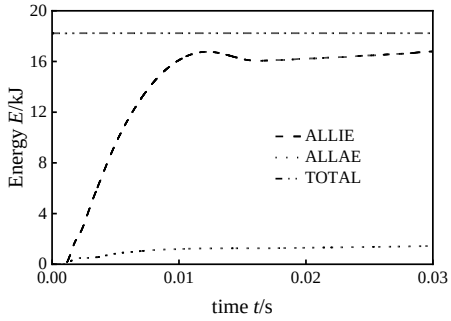

Figure 4. The energy–time history curve.

In order to further ensure the reliability of this numerical model, some column specimens provided in the literature [7,21] are selected for comparison. The numerical simulation results, which contain the overall damage pattern of the CFDST column and the time history of impact force and mid-span deflection, are compared with the test ones. The specimens are listed in Table 3. With regard to the labels in Table 3, L stands for the length of the specimen; D, t, and f_y stand for the section diameter, the thickness, and the yield strength of the steel tube, in which the subscript "o" stands for the outer steel tube while the subscript "i" stands for the inner one; f_{cu} stands for the cubic compressive strength of concrete; m_0 stands for the impact mass; v_0 stands for the impact velocity; and n stands for the ratio of axial compression.

Table 3. The specimens for verification.

Specimen	L/mm	$D_o \times t_o$	$D_i \times t_i$	f_{cu}/MPa	f_{yo}/MPa	f_{yi}/MPa	m_0/kg	v_0/(m/s)	n
s-FF3-0.15	1500	170 × 2	100 × 3	60.2	396	389	229.8	7.6	0.15
s-FF5-0.15	1500	170 × 2	100 × 3	60.2	396	389	229.8	9.8	0.15
s-FF7-0.15	1500	170 × 2	100 × 3	60.2	396	389	229.8	10.8	0.15
CCFPIP-1-1	2000	219.1 × 10	139.7 × 5	63.8	400	420	1350	7.56	0
CCFPIP-5-1	2000	219.1 × 6.3	139.7 × 6.3	60.6	395	395	1350	7.65	0
CCFPIP-7-1	2000	219.1 × 6.3	168.3 × 6.3	60.6	395	395	1350	7.72	0

The test and numerical damage patterns are shown in Figure 5. The specimens show overall bending deformation with local buckling at the top of the mid-span of the specimen. The numerical model can simulate the damage pattern of the CFDST column under the coupling action of axial compression and lateral impact well.

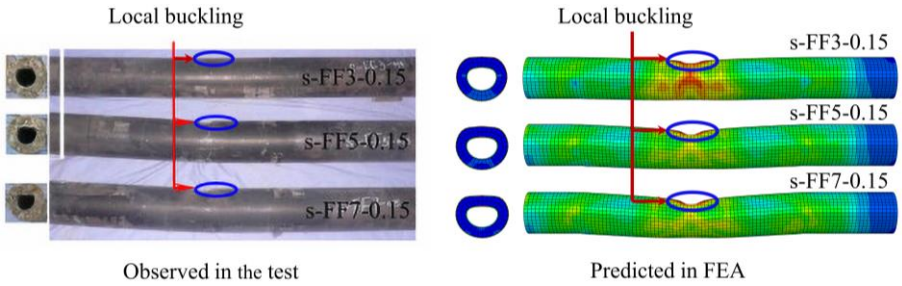

Figure 5. The damage pattern.

Figure 6 presents the comparisons between the test and numerical results in terms of the impact force and the mid-span deflection curves of the CFDST column. Both the impact force and mid-span deflection curves have high accuracy in terms of overall trend and duration. When the contact between the impact mass and the column takes place, the impact mass penetrates the column immediately and leads to the first peak impact force. Following the peak impulse, the impact force curve vibrates around the plateau value, F_{stab}. During the whole process, the peak impact force is named F_{max}. The mid-span deflection curves rise to the peak value, u_{max}, when the impact contact takes place, and then turn to descend to a residual value, u_{stab}. The specific values of these four parameters are shown in Table 4. Compared with the test results, the errors of the numerical results are all less than 10%. It can be seen that the numerical model established in this paper is in good agreement with the test, and can be further used to accurately analyze the dynamic responses of the CFDST column under the coupling action of axial compression and lateral impact.

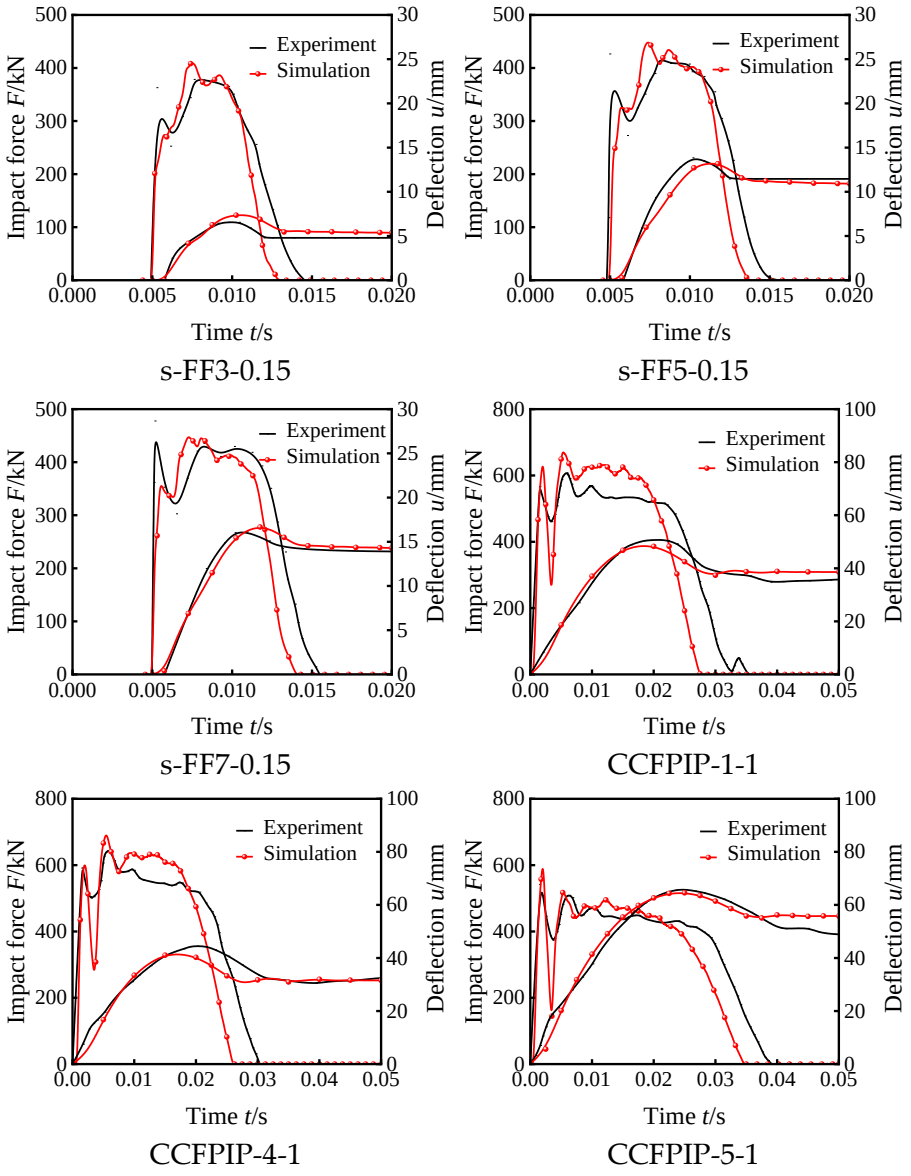

Figure 6. Comparison of numerical and test curves.

Table 4. Comparison of numerical and test results.

Specimen	F_{max}/kN			F_{stab}/kN			u_{max}/mm			u_{stab}/mm		
	Numerical	Test	Error/%	Numerical	Test	Error/%	Numerical	Test	Error/%	Numerical	Test	Error/%
s-FF3-0.15	409	374	9	376	380	−1	6.6	7.4	−10	5.4	5.4	0
s-FF5-0.15	449	432	4	419	390	7	13.8	13.2	5	11.5	11	5
s-FF7-0.15	449	442	2	420	385	9	16.1	16.7	−4	13.8	14.4	−4
CCFPIP-1-1	639	606	5	602	545	10	50.8	48.6	−5	——	——	——
CCFPIP-4-1	693	644	8	605	572	6	44.6	41.6	−7	——	——	——
CCFPIP-5-1	604	546	10	458	451	2	65.9	64.6	−2	——	——	——

3. Parameter Analysis

3.1. Specimen Design

The numerical model of the CFDST column under the coupling action of axial compression and lateral impact is developed based on the above process. A basic column specimen is designed with the length L = 1800 mm, the diameters of the outer and inner steel tube D_o = 180 mm and D_i = 88 mm, the thickness of outer and inner steel tube $t_o = t_i$ = 3 mm, the compressive strength of concrete f_c = 60 MPa, and the yield strength of steel f_y = 396 MPa. The rigid mass of lateral impact is m = 450 kg, and the initial velocity is v_0 = 7 m/s. Depending on the basic member, a series of CFDST columns are designed by varying the diameter of the inner steel tube, the length, the strength of concrete and steel, the spring compression displacement, and the impact velocity. The effects of hollow ratio, axial compression ratio, slenderness ratio, material strength, and impact energy on the dynamic responses of the CFDST column under the coupling action are studied.

The column specimens with their specific parameters are listed in Table 5, in which the basic specimen is named S-5374. The specimens are named with four parameters, which are the hollow ratio χ, the axial compression ratio n, the impact velocity v_0, and the slenderness ratio λ in order. The hollow ratio is defined as [22]

$$\chi = \frac{D_i}{D_o - 2t_o} \tag{6}$$

Table 5. Specimens and responses.

Specimen	$D_i \times t_i$ (mm)	L (mm)	χ	n	v_0 (m·s^{-1})	λ	f_c (MPa)	f_{yo} (MPa)	f_{yi} (MPa)	N_u (kN)	F_{max} (kN)	F_{stab} (kN)	u_{max} (mm)	u_{stab} (mm)
S-3374	52 × 3	1800	0.3	0.3	7	40	60	396	396	1964	569	267	34.1	30.3
S-5374	88 × 3	1800	0.5	0.3	7	40	60	396	396	1894	439	295	26.7	22.9
S-7374	120 × 3	1800	0.69	0.3	7	40	60	396	396	1743	370	296	18.9	14.8
S-8374	140 × 3	1800	0.8	0.3	7	40	60	396	396	1604	277	240	8.6	6.7
S-5174	88 × 3	1800	0.5	0.15	7	40	60	396	396	1894	440	292	27.2	23.3
S-5474	88 × 3	1800	0.5	0.45	7	40	60	396	396	1894	432	283	28.1	23.7
S-5674	88 × 3	1800	0.5	0.6	7	40	60	396	396	1894	421	269	29.6	26.2
S-5334	88 × 3	1800	0.5	0.3	3	40	60	396	396	1894	323	248	6.4	2.9
S-5354	88 × 3	1800	0.5	0.3	5	40	60	396	396	1894	341	285	14.5	10.5
S-5394	88 × 3	1800	0.5	0.3	9	40	60	396	396	1894	522	295	44.9	41.1
S-5373	88 × 3	1350	0.5	0.3	7	30	60	396	396	1894	475	435	15.2	13.1
S-5375	88 × 3	2250	0.5	0.3	7	50	60	396	396	1894	440	223	38.5	32.8
S-5376	88 × 3	2700	0.5	0.3	7	60	60	396	396	1894	442	163	52.4	44.6
S-5374-C20	88 × 3	1800	0.5	0.3	7	40	20	396	396	1312	406	275	28.8	24.2
S-5374-C40	88 × 3	1800	0.5	0.3	7	40	40	396	396	1601	423	282	27.7	23.6
S-5374-C80	88 × 3	1800	0.5	0.3	7	40	80	396	396	2180	457	305	26.2	22.6
S-5374-300	88 × 3	1800	0.5	0.3	7	40	60	300	300	1646	402	232	34.4	31.2
S-5374-350	88 × 3	1800	0.5	0.3	7	40	60	350	350	1775	420	267	29.7	26.2
S-5374-400	88 × 3	1800	0.5	0.3	7	40	60	400	400	1901	454	300	26.6	23.1
S-5374-450	88 × 3	1800	0.5	0.3	7	40	60	450	450	2033	452	327	24.1	20.0

The axial compression ratio, n, is defined as [7]

$$n = \frac{N_0}{N_u} \tag{7}$$

where N_0 is the actual vertical load applied to the column and N_u is the ultimate bearing capacity of the CFDST column under axial compression, which is calculated as [23]

$$N_u = N_{i,u} + N_{osc,u} \quad (8)$$

where $N_{i,u}$ is the ultimate bearing capacity of the inner steel tube and $N_{osc,u}$ is the ultimate bearing capacity of the outer steel tube and concrete.

The dynamic responses of the column specimens are listed in Table 5 as well, including the values of impact force and mid-span deflection.

3.2. Influence of Hollow Ratio

To analyze the influence of the hollow ratio on the dynamic responses of the CFDST column under lateral impact, four specimens (S-3374, S-5374, S-7374, and S-8374) with hollow ratios of 0.3, 0.5, 0.69, and 0.8 are designed by keeping the size of outer steel tube constant and varying the inner one. Under the lateral impact, the peak impact force shows a decreasing trend with the hollow ratio ranging from 0.3 to 0.8, as indicated in Table 5. Compared to specimen S-3374 (χ = 0.3), the peak impact force of specimen S-8374 (χ = 0.8) decreases by almost 51.3%. However, the plateau impact force shows an increasing trend following a decreasing one, as shown in Figure 7a. The reason may be that the specimen's empty steel tube would bend, and the concrete's supporting effect on the steel tube is weakened when the hollow ratio exceeds a certain range.

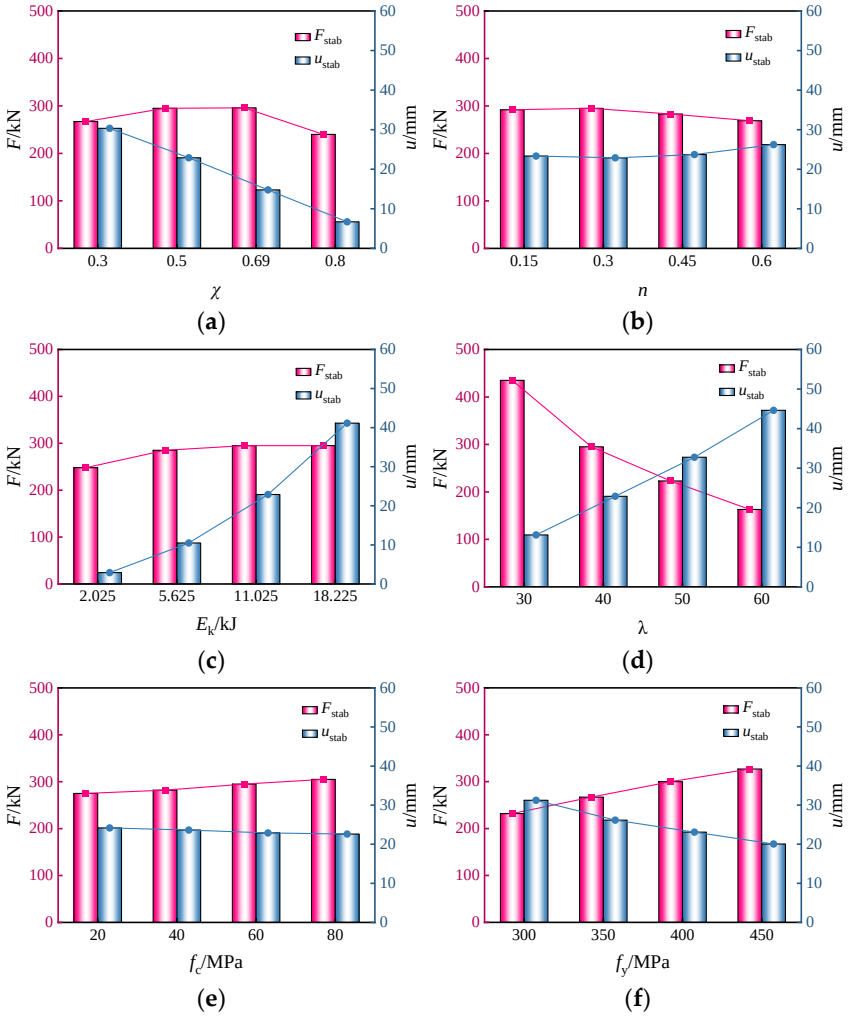

Figure 7. Dynamic responses of the CFDST columns. (**a**) Hollow ratio. (**b**) Axial compression ratio. (**c**) Impact energy. (**d**) Slenderness ratio. (**e**) Concrete strength. (**f**) Steel strength.

The mid-span deflection shows a decreasing trend as listed in Table 5. Compared to specimen S-3374, the peak mid-span deflection of specimen S-8374 decreases by almost 74.8%, and the residual mid-span deflection decreases by 77.9%. With the increase in the hollow ratio, the main deformation model of the column changes from overall bending to local depression at the impact site, and the failure patterns of the cross-sections are shown in Figure 8.

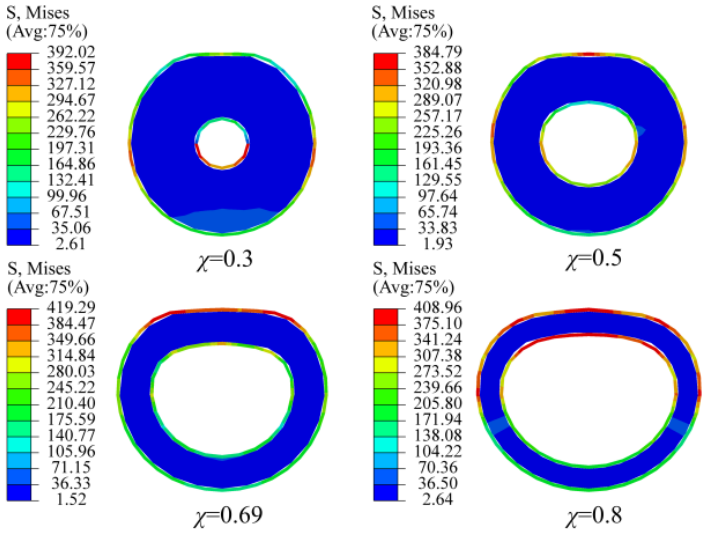

Figure 8. Failure pattern of the cross section.

3.3. Influence of Axial Compression Ratio

To analyze the influence of axial compression ratio, four specimens (S-5174, S-5374, S-5474, and S-5674) with axial compression ratios of 0.15, 0.3, 0.45, and 0.6 are designed by varying the compression displacement of the axial spring. As indicated in Figure 7b, the change in impact force increases slightly when the ratio is less than 0.3, while it decreases clearly when higher than 0.3. Compared to specimen S-5374 (n = 0.3), the impact force of specimen S5674 (n = 0.6) decreases by almost 4.1% and 8.8% for peak and plateau values. This is because the concrete is in the confined stress state when the axial compression state is relatively low, which can improve the performance of the column slightly. However, when the axial compression state is relatively high, the axial compression accelerates the overall bending deformation of the members under lateral impact.

The mid-span deflection shows an increasing trend following a decreasing one, as listed in Table 5. Compared to specimen S-5374, the peak mid-span deflection of specimen S-5674 increases by almost 10.9%, and the residual mid-span deflection increases by 14.4%.

3.4. Influence of Impact Energy

To analyze the influence of impact energy, four specimens (S-5334, S-5354, S-5374, and S-5394) with impact velocities of 3 m/s, 5 m/s, 7 m/s, and 9 m/s are designed. The impact force shows an increasing trend with the impact energy, as indicated in Figure 7c. Compared to specimen S-5334 (v_0 = 3 m/s), the plateau impact force of specimen S-5394 (v_0 = 9 m/s) increases by almost 52.6%. With the increase in impact energy, the mid-span deflection increases significantly. Compared to specimen S-5334, the residual mid-span deflection of specimen S-5394 increases about 13 times. That is because the column absorbs more plastic strain energy in the plastic deformation stage.

3.5. Influence of Slenderness Ratio

To analyze the influence of slenderness ratio, four specimens (S-5373, S-5374, S-5375, and S-5376) with slenderness ratios of 30, 40, 50, and 60 are designed. As indicated in Table 5, the slenderness ratio has almost no effect on the peak impact force, but has a

significant effect on the plateau impact force. With the increase in slenderness ratio from 30 to 60, the plateau impact force decreases by almost 62.5%. As shown in Figure 7d, the mid-span deflection increases significantly with the increase in slenderness ratio as well. Compared to specimen S-5373, the peak and residual mid-span deflections of specimen S-5376 increase by 244.7% and 240.5%, respectively. This is because the restraint of the two ends of the column has less effect on the dynamic responses with the slenderness ratio increasing.

3.6. Influence of Concrete Strength

To analyze the influence of concrete strength, four specimens with concrete strengths of 20 MPa, 40 MPa, 60 MPa, and 80 MPa are designed. As indicated in Table 5, the peak impact force increases linearly with the increase in concrete strength, and the same is true for the plateau impact force. With the increase in concrete strength, the mid-span deflection of the specimen shows a decreasing trend, but the range of variation is only about 2 mm.

3.7. Influence of Steel Strength

To analyze the influence of steel strength, four specimens with steel strengths of 300 MPa, 350 MPa, 400 MPa, and 450 MPa are designed. As indicated in Table 5, the increase in the steel strength can effectively improve the impact force. With the increase in steel strength, the mid-span deflection of the specimen shows a decreasing trend, and the range of variation is wider compared to the concrete.

To sum up, with the increase in the hollow ratio from 0.3 to 0.8, the residual mid-span deflection of CFDST column decreases by 77.9%. The main deformation model of the column changes from overall bending to local depression at the impact site. The mid-span deflection shows an increasing trend following a decreasing one with the axial compression ratio increasing. The axial compression accelerates the overall bending deformation of the column under lateral impact when the axial compression state is relatively high. With the increase in the slenderness ratio from 30 to 60, the plateau impact force decreases by 62.5%, and the residual mid-span deflection increases by 240.5%. The increase in the material strength and impact energy can also increase the impact force to varying degrees. Referring to the relevant literature [4,24], the plateau impact force is regarded as the impact-bearing capacity, and the residual mid-span deflection is an important index to characterize the deformation ability of the specimen.

4. Practical Formulas

Based on the parameter analysis of the dynamic responses, the practical formula for the impact-bearing capacity of the CFDST column is suggested as

$$F_d = F_{\text{stab}} = (0.3065K + 0.0185)F_s \tag{9}$$

$$K = f(\chi)f(n)f(E_{\text{k}})f(\lambda)f(f_{\text{c}})f(f_{\text{y}}) \tag{10}$$

where the static flexural bearing capacity of the column, F_{s}, is obtained from the literature [19]. The influence coefficients of each parameter on the impact-bearing capacity, f, are shown below:

$$f(\chi) = -2.6309\chi^2 + 2.0361\chi + 0.9258$$

$$f(n) = -0.8064n^2 + 0.3816n + 1.2093$$

$$f(E_{\text{k}}) = -0.0017{E_{\text{k}}}^2 + 0.0446E_{\text{k}} + 0.9885$$

$$f(\lambda) = -0.0111\lambda + 1.7226$$

$$f(f_{\text{c}}) = -0.0042f_{\text{c}} + 1.5213$$

$$f(f_{\text{y}}) = -5 \times 10^{-6}{f_{\text{y}}}^2 + 0.0041f_{\text{y}} + 0.3893$$

The practical formula for the residual mid-span deflection of the CFDST column is suggested as

$$u_{\text{stab}} = 5.0207S - 138.8 \text{ (mm)} \tag{11}$$

$$S = g(\chi)g(n)g(E_{\text{k}})g(\lambda)g(f_{\text{c}})g(f_{\text{y}}) \tag{12}$$

where the influence coefficients of each parameter on the residual mid-span deflection, g, are shown below:

$$g(\chi) = -45.901\chi + 44.956$$

$$g(n) = 32.943n^2 - 18.357n + 25.372$$

$$f(E_{\text{k}}) = 2.3674E_{\text{k}} - 2.4838$$

$$g(\lambda) = 1.0436\lambda - 18.61$$

$$g(f_{\text{c}}) = -0.0271f_{\text{c}} + 24.683$$

$$g(f_{\text{y}}) = -0.0733f_{\text{y}} + 52.626$$

in which the unit of E_{k} is kJ, and the units of f_{c} and f_{y} are both MPa. The validity limits of Equations (9)–(12) are shown in Table 6.

Table 6. Parameter range of formula.

Impact Position	χ	n	λ	E_{k}/kJ	f_{c}/MPa	f_{y}/MPa
Mid-span	0.3~0.8	0.15~0.6	30~60	2.025~18.225	20~80	300~450

As shown in Figure 9, the calculated values of the dynamic increase factor of impact-bearing capacity (DIF = $F_{\text{d}}/F_{\text{s}}$) and residual mid-span deflection u_{stab} from the practical formulas are compared with the simulated ones. The relative errors between these two sets of values are less than 5%. The practical formulas are accurate enough to guide the design of the CFDST column.

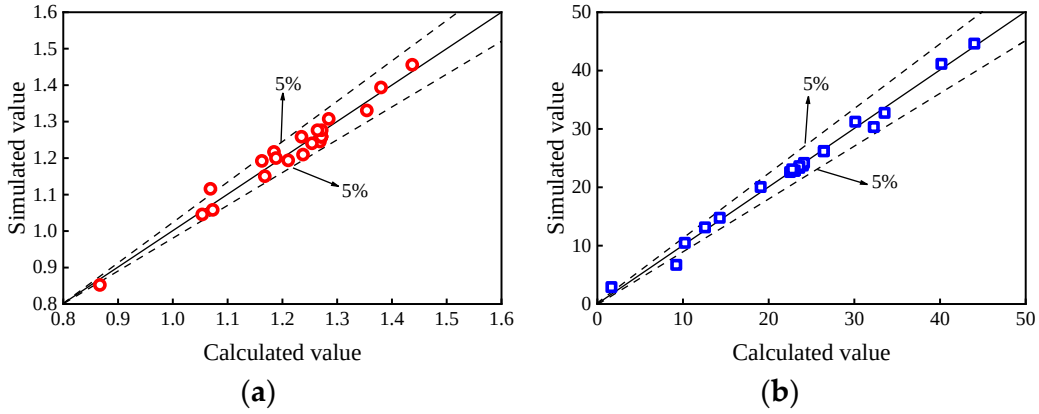

Figure 9. Comparison of calculated and simulated values. (**a**) DIF. (**b**) u_{stab}/mm.

5. Conclusions

A numerical model is established in this paper, and the dynamic responses of the CFDST column under the coupling action of axial compression and lateral impact are analyzed. The results are summarized below:

(1) The numerical model established in this paper can be used to accurately analyze the dynamic responses of the CFDST column under the coupling action of axial force and lateral impact. The axial compression state of the column can be simulated by importing the result of static analysis into this explicit model as an initial stress field.

(2) With the increase in the hollow ratio from 0.3 to 0.8, the residual mid-span deflection of the CFDST column decreases by 77.9%. The main deformation model of the

column changes from overall bending to local depression at the impact site. The mid-span deflection shows an increasing trend following a decreasing one with the axial compression ratio increasing. The axial compression accelerates the overall bending deformation of the column under lateral impact when the axial compression state is relatively high. With the increase in the slenderness ratio from 30 to 60, the plateau impact force decreases by 62.5%, and the residual mid-span deflection increases by 240.5%. The increase in the material strength and impact energy can also increase the impact force to varying degrees.

(3) The practical formulas for impact-bearing capacity and residual mid-span deflection of the CFDST column under lateral impact are accurate enough in the validity limits. The formula for impact-bearing capacity could be used to guide the design of CFDST columns under lateral impact, and the formula for residual mid-span deflection could also be significant for the failure criterion of CFDST columns under lateral impact.

Author Contributions: Conceptualization, J.-L.G.; methodology, J.-L.G.; software, S.P.; validation, J.-L.G. and S.P.; formal analysis, S.P.; investigation, X.G. and Z.-Y.W.; resources, J.-L.G. and X.G.; data curation, J.-L.G. and S.P.; writing—original draft preparation, J.-L.G. and S.P.; writing—review and editing, J.-L.G. and Z.-Y.W. All authors have read and agreed to the published version of the manuscript.

Funding: This research was funded by the National Natural Science Foundation of China (No. 52104122), Fujian Province Natural Sciences (2020J01943), and Fujian Jiangxia University Scientific Foundation (JXZ2019003).

Data Availability Statement: The data presented in this study are available on request from the corresponding author.

Acknowledgments: The authors are grateful to the Institute of Infrastructural Protection in Fujian Jiangxia University for the financial grant.

Conflicts of Interest: The authors declare no conflict of interest.

References

1. Huang, H.; Qi, B.H.; Wang, H.Z. Axial compressive behavior of ultra-high performance concrete short columns with large hollow ratio circular hollow sandwich steel tube. *Prog. Steel Build. Struct.* **2022**, *24*, 24–31, 46.
2. Yu, X.; Tao, Z. Experimental study on residual bearing capacity of hollow sandwich concrete-filled steel tubular short axial compression column after fire. *Ind. Archit.* **2009**, *39*, 9–13.
3. Sulthana, U.M.; Jayachandran, S.A. Axial compression behaviour of long concrete filled double skinned steel tubular columns. *Structures* **2017**, *9*, 157–164.
4. Hou, C.C. Study on Performance of Circular Concrete-Filled Steel Tubular (CFST) Members under Low Velocity Transverse Impact. Master's Thesis, Tsinghua University, Beijing, China, 2012.
5. Feng, Z.J.; Wang, X.L.; Zhang, S.F. Experimental investigation on cantilever square CFST columns under lateral continuous impact loads. *J. Constr. Steel Res.* **2022**, *196*, 107416. [CrossRef]
6. Wang, W.D.; Zheng, L.; Xian, W. Performance of the CFST column to composite beam connection under static and impact loads. *J. Constr. Steel Res.* **2022**, *198*, 107567. [CrossRef]
7. Wang, R.; Han, L.H.; Zhao, X.L. Experimental behavior of concrete filled double steel tubular (CFDST) members under low velocity drop weight impact. *Thin-Walled Struct.* **2015**, *97*, 279–295. [CrossRef]
8. Shi, Y.; Li, X.Y.; Zhang, J.B. Experimental study on lateral impact of hollow sandwich metal tube concrete members. *J. Vib. Meas. Diagn.* **2020**, *40*, 982–988.
9. Wang, B.B.; Wang, R. Effect of hollow ratio on crash worthiness of stainless steel concrete steel double-skin tubular columns. *Explos. Shock. Waves* **2018**, *38*, 204–211.
10. An, G.Q.; Zhao, H.; Wang, R. Calculation method for impact resistance of circular concrete-filled double-skin tubular columns with external stainless steel tube. *Eng. Mech.* **2021**, *38*, 227–236.
11. Aghdamy, S.; Thambiratnam, D.P.; Dhanasekar, M. Effects of structure-related parameters on the response of concrete-filled double-skin steel tube columns to lateral impact. *Thin-Walled Struct.* **2016**, *108*, 351–368. [CrossRef]
12. Kang, L.J.; Fan, W.; Liu, B. Numerically efficient analysis of concrete-filled steel tubular columns under lateral impact loading. *J. Constr. Steel Res.* **2021**, *179*, 106564. [CrossRef]
13. Jahami, A.; Temsah, Y.; Khatib, J. The behavior of CFRP strengthened RC beams subjected to blast loading. *Mag. Civ. Eng.* **2021**, *103*, 10309.

14. Wu, H.; Peng, Y.L.; Fang, Q. Experimental and numerical study of ultra-high performance cementitious composites filled steel tube (UHPCC-FST) subjected to close-range explosion. *Int. J. Impact Eng.* **2020**, *141*, 103569. [CrossRef]
15. Han, L.H.; Yao, G.H.; Tao, Z. Performance of concrete filled thin-walled steel tubes under pure torsion. *Thin-Walled Struct.* **2007**, *45*, 24–36. [CrossRef]
16. American Concrete Institute. *Building Code Requirement for Structural Concrete and Commentary: ACI Committee 318(ACI 318)*; American Concrete Institute: Detroit, MI, USA, 2005.
17. Cai, J.; Yu, Y.; Chen, Q.J. Parameter study on dynamic response of concrete filled square tube under lateral impact. *J. Cent. S. Univ.* **2019**, *50*, 409–419.
18. Zeinoddini, M.; Parke, G. A. R.; Harding, J. E. Axially pre-loaded steel tubes subjected to lateral impacts: An experimental study. *Int. J. Impact Eng.* **2002**, *27*, 669–690. [CrossRef]
19. Wang, R.; Han, L.H.; Zhao, X.L. Analytical behavior of concrete filled double steel tubular (CFDST) members under lateral impact. *Thin-Walled Struct.* **2016**, *101*, 129–140. [CrossRef]
20. Kang, C.M.; Wang, R.; Zhu, X. The influence of axial compression ratio on the lateral impact performance of concrete filled steel tube columns. *Eng. Mech.* **2020**, *37*, 254–260.
21. Wang, Y.; Qian, X.D.; Liew, J.Y.R. Experimental behavior of cement filled pipe-in-pipe composite structures under transverse impact. *Int. J. Impact Eng.* **2014**, *72*, 1–16. [CrossRef]
22. Han, L.H.; Li, Y.J.; Liao, F.Y. Concrete-filled double skin tubular (CFDST) columns subjected to long-term sustained loading. *Thin-Walled Struct.* **2011**, *49*, 1534–1543. [CrossRef]
23. Han, L.H.; Huang, H.; Tao, Z. Concrete-filled double skin steel tubular (CFDST) beam-columns subjected to cyclic bending. *Eng. Struct.* **2006**, *28*, 1698–1714. [CrossRef]
24. Guo, J.L.; Cai, J.; Zuo, Z.L. Simplified Dynamic Analysis of Reinforced Concrete Beams under Impact Actions. Proceedings of the Institution of Civil Engineers. *Struct. Build.* **2017**, *170*, 211–224. [CrossRef]